Journal of Inorganic Biochemistry xxx (xxxx) 111433

Contents lists available at ScienceDirect

Journal of Inorganic Biochemistry

journal homepage: www.elsevier.com/locate/jinorgbio

Combinatorial delivery of doxorubicin and acridine orange by gold core silica shell nanospheres functionalized with poly(ethylene glycol) and 4-methoxybenzamide for cancer targeted therapy

Rafaela S. Guimarães [a], Carolina F. Rodrigues [a], Natanael Fernandes [a], Duarte de Melo-Diogo [a], Paula Ferreira [b], Ilídio J. Correia [a, b, *], André F. Moreira [a, *]

[a] CICS-UBI – Health Sciences Research Centre, Universidade da Beira Interior, Av. Infante D. Henrique, 6200-506 Covilhã, Portugal
[b] CIEPQPF — Departamento de Engenharia Química, Universidade de Coimbra, Rua Sílvio Lima, 3030-790 Coimbra, Portugal

ARTICLE INFO

Editor name: John Dawson

Keywords:
Cancer
Drug combination
Acridine orange
Doxorubicin
Gold core silica shell nanoparticles
PEG
Anisamide

ABSTRACT

Combinatorial therapies based on the simultaneous administration of multiple drugs can lead to synergistic effects, increasing the efficacy of the cancer therapy. However, it is crucial to develop new delivery systems that can increase the drugs' therapeutic selectivity and efficacy. Gold core silica shell (AuMSS) nanoparticles present physicochemical properties that allow their simultaneous application as drug delivery and imaging agents. Herein, poly(ethylene glycol) was modified with 4-methoxybenzamide and 3-(triethoxysilyl)propyl isocyanate (TPANIS) to create a novel surface functionalization capable of improving the colloidal stability and specificity of AuMSS nanospheres towards cancer cells. Moreover, a dual drug combination based on Doxorubicin (DOX) and Acridine orange (AO) was characterized and administered using the AuMSS-TPANIS nanospheres. The obtained results show that the DOX:AO drug combination can mediate a synergistic therapeutic effect in both HeLa and MCF-7 cells, particularly at the 2:1, 1:1, and 1:2 ratios. Otherwise, the TPANIS functionalization increased the AuMSS nanospheres colloidal stability and selectivity towards MCF-7 cancer cells (overexpressing sigma receptors). Such also resulted in an enhanced cytotoxic effect against MCF-7 cells when administering the DOX:AO drug combination with the AuMSS-TPANIS nanospheres. Overall, the obtained results confirm the therapeutic potential of the DOX:AO drug combination as well as the targeting capacity of AuMSS-TPANIS, supporting its application in the cancer-targeted combinatorial chemotherapy.

1. Introduction

Cancer is a major health problem worldwide and it is responsible for millions of deaths every year [1,2]. Chemotherapy is one of the most used anticancer therapies despite its low therapeutic efficacy and side effects. Such can be explained by rapid degradation, low solubility and selectivity of chemotherapeutic drugs to cancer cells [3,4]. Additionally, cancer cells can develop resistance to multiple drugs, which highlights the demand for new and more effective anti-cancer approaches [5,6]. Combinatorial therapies based on the simultaneous administration of multiple drugs can lead to synergistic effects, that increase the therapeutic efficiency of chemotherapy [7,8]. The rationale underlying the development/testing of drug combinations has been to co-administer drugs that act on different targets to overcome the multidrug resistance mechanisms and consequently increase the elimination of cancer cells [9]. Additionally, such therapeutic modality allows the reduction of the drug doses and minimizes the drug-associated side-effects [10–12]. However, the occurrence of antagonistic effects and the different pharmacokinetic profiles of the drugs can lead to a decrease in the antitumoral efficacy of combinatorial therapies [4,13]. To further improve the selectivity and efficacy, while decreasing their systemic toxicity, it is crucial to develop new delivery systems. Among the drug delivery systems that have been developed so far, gold core silica shell (AuMSS) nanoparticles present excellent physicochemical and biological properties that allow their simultaneous application in chemotherapy and bioimaging [14–16]. In these nanomaterials, the gold core can act as a contrast agent for bioimaging applications, whereas the well-defined porous structure of mesoporous silica can act

* Corresponding authors at: CICS-UBI – Health Sciences Research Centre, Universidade da Beira Interior, Av. Infante D. Henrique, 6200-506 Covilhã, Portugal.
E-mail addresses: icorreia@ubi.pt (I.J. Correia), afmoreira@fcsaude.ubi.pt (A.F. Moreira).

https://doi.org/10.1016/j.jinorgbio.2021.111433
Received 5 November 2020; Received in revised form 15 March 2021; Accepted 17 March 2021
0162-0134/

as a reservoir of different pharmaceutical agents (*e.g.* drugs, genes, antibodies), for protecting them from premature degradation and avoiding their interaction with healthy tissues [17–19]. Additionally, the silica shell possesses a high surface area that can be easily modified with different polymers and molecules, to avoid the immune system recognition, promote the tumor targeting, and confer a stimuli-responsive behaviour [20,21].

In this work, a dual drug combination based on doxorubicin (DOX) and acridine orange (AO) was encapsulated in AuMSS nanospheres. DOX is an anthracycline drug widely used for the treatment of different types of cancer, which interact with DNA by intercalation between neighbouring base pairs through covalent and hydrogen bonds, thus preventing DNA replication and ultimately the protein synthesis [22]. Additionally, DOX also inhibits the topoisomerase II (Top II), an enzyme that can regulate the DNA condensation, relaxing the accumulated positive supercoils, as well as untangling the intertwined DNA strands [23]. On the other hand, AO is a basic weak dye that is also used as a pH indicator, photosensitizer, antitumoral drug, antibacterial and antiparasitic agent [24–26]. AO has been recently applied in cancer therapy due to its preferential accumulation in acidic environments, such as the cancer tissue, and due to its intercalation within the double helix of DNA or by electrostatic attraction to the negatively charged phosphate groups (DNA and RNA) [26–29]. Additionally, the AO low molecular weight facilitates its diffusion into the cytoplasm of the cells as well as binding to DNA, RNA, and acidic vesicles (*e.g.* lysosomes) [24,25].

To create a novel surface functionalization for the AuMSS nanospheres, poly(ethylene glycol) (PEG) was modified with 4-Methoxybenzamide (ANIS) and 3-(triethoxysilyl)propyl isocyanate (TESPIC). The ANIS was selected due to its specificity for sigma-1 receptors that are overexpressed in some cancers (*e.g.* melanoma, breast, lung, and prostate cancer) [30–32]. Therefore, this ligand can improve the nanoparticles' selectivity to cancer cells reducing the nonspecific distribution. On the other hand, PEG was selected due to its amphiphilic nature and high solubility, which reduce protein adsorption on nanoparticles' surface, and consequently increase its blood circulation time [33,34]. The functionalization of AuMSS nanospheres was achieved through a post-synthesis methodology. Moreover, the therapeutic potential of the DOX:AO drug combination and AuMSS-TPANIS nanospheres cancer-targeted combinatorial chemotherapy were characterized in breast and cervical cancer cell lines.

2. Experimental section

2.1. Materials

Hydrogen tetrachloroaurate (III) hydrate ($HAuCl_4$–99.9% (metals basis), Au 49% min) was obtained from Alfa Aesar (Germany). Tetraethyl orthosilicate (TEOS – purity > 97%), tetrahydrofuran anhydrous (THF) stabilized with BHT, and hexadecyltrimethylammonium bromide (CTAB – purity 98%) were acquired from Tokyo Chemical Industry (Japan). Hydrochloric acid (HCl), methanol and ethanol (EtOH) were obtained from VWR International (Carnaxide, Portugal). Dulbecco's Modified Eagle medium-high glucose (DMEM-HG), Dulbecco's Modified Eagle Medium: Nutrient Mixture F-12 (DMEM-F12) resazurin, formaldehyde (37 wt% in H_2O), trypsin, AO (purity > 98%), fluorescein isothiocyanate (FITC), phosphate-buffered saline (PBS) solution, TESPIC, PEG (Mw: 10 000 g/mol), dichloromethane anhydrous (DCM – ≥99.8%), and ANIS (Mw: 151.16 g/mol) were purchased from Sigma–Aldrich (Sintra, Portugal). Fetal bovine serum (FBS) was acquired to Biochrom AG (Berlin, Germany). Primary Normal Human Dermal Fibroblasts (FibH) cells were acquired from PromoCell (Labclinics, S.A., Barcelona, Spain). Human negroid cervix epithelioid carcinoma (HeLa, passage number 10–15) cells (ATCCs CCL-2 t) and Michigan Cancer Foundation-7 (MCF-7, passage number 8–10) cells were purchased from ATCC (Middlesex, UK). Doxorubicin hydrochloride (DOX – purity > 98%) was obtained from Carbosynth (Berkshire, UK). Cell culture t-flasks were obtained from Orange Scientific (Braine-l'Alleud, Belgium). Cell imaging plates were acquired from Ibidi GmbH (Munich, Germany).

2.2. Methods

2.2.1. Cytotoxic activity of DOX and AO in cell culture

The cytotoxicity profile of DOX and AO in HeLa and MCF-7 cells was evaluated through a resazurin-based assay [14]. For that purpose, HeLa or MCF-7 cells were seeded in 96-well culture plates with DMEM-HG or DMEM-F12 culture medium, respectively, at a density of 10,000 cells/well. After 24 h, the cells were incubated with increasing drug concentrations for 48 h. Then, the medium was replaced with the resazurin solution and incubated 4 h at 37 °C and 5% CO_2. The cell viability was determined by measuring the resorufin fluorescence by using a microwell plate reader (Spectramax Gemini XS, Molecular Devices LLC, USA) at an excitation/emission wavelength of $\lambda ex = 560$ nm and $\lambda em = 590$ nm. Cells incubated with EtOH were used as a positive control (K^+), whereas non-incubated cells were used as a negative control (K^-). Posteriorly, OriginLab software (trial version, OriginPro, OriginLab Corporation, MA, USA) was used to trace the drugs' dose-response curves and determine the DOX and AO inhibitory concentrations (ICs), *i.e.*, IC_{20}, IC_{50}, and IC_{80} (*i.e.*, concentrations producing 20, 50, and 80% reduction in cell viability) [35].

2.2.2. Screening of DOX:AO combinations

After calculating the ICs of DOX and AO, different DOX and AO combination ratios (DOX:AO) were tested in HeLa cancer cells. Briefly, the cells were seeded in 96-well culture plates at a density of 10,000 cells/well and cultured for 24 h at 37 °C and 5% CO_2. After this period, different drug ratios were incubated for 48 h. The overall tested drug concentration was equivalent to the IC_{20}, IC_{50}, and IC_{80} calculated for DOX (please see Table S1 of supporting information). Subsequently, the 3 most promising drug ratios were selected and the dose-response curves and IC_{20}, IC_{50}, and IC_{80} values were determined for each drug ratio (please see section 2.2.1.) in both HeLa and MCF-7 cancer cells. Additionally, the Combination Index (CI) of the different drug ratios was determined using the Chou-Talalay method at inhibition levels of 20, 50, and 80% [36,37]. Drug ratios with CI values lower than 1 were considered synergistic, whereas CI values higher than 1 were considered antagonistic.

2.2.3. Synthesis of AuMSS nanospheres

AuMSS nanospheres were synthesized through a method previously described in the literature [38]. Initially, gold spherical cores were produced by adding 1 mL of formaldehyde (3.7%) and 0.8 mL of $HAuCl_4$ (0.05 M) to a solution composed of 0.05 g of CTAB, 0.6 mL of NaOH (0.5 M), and 24 mL of ultrapure water. After 10 min at 80 °C, 910 μL of TEOS (33% *v*/v in methanol) were added to the previous solution and reacted for 1 h. The AuMSS nanospheres were recovered by centrifugation at 11000*g* and 25 °C. Posteriorly, the highly cytotoxic CTAB surfactant template was removed from nanoparticles by adapting a solvent-based approach described in the literature [39]. Briefly, several washing steps were performed by resuspending the AuMSS nanorods in an HCl (7.5% *v*/v in EtOH) solution, followed by sonication for 5 min, and centrifugation (18,000 *g*, 20 min at 25 °C). Then, the purified AuMSS nanorods were recovered by centrifugation (18,000 *g* for 15 min) and resuspended in ultrapure water.

2.2.4. Synthesis of TESPIC-PEG-ANIS

The reaction of PEG and ANIS was performed by adapting an approach described in the literature [40]. PEG (0.5 mmol) was dissolved in 3 mL of dry DCM under a nitrogen atmosphere and magnetic stir-

ring. Then, 1,1′-carbonyldiimidazole (CDI) (89.1 mg) was added dropwise to the previous solution and allowed to react under nitrogen atmosphere for 6 h. Subsequently, ANIS (151.6 mg) was dissolved in 6 mL of EtOH (100% *v*/v) and added to the activated PEG. After 14 h, the solvent was removed by evaporation (Rotavap®R-215, Büchi, Switzerland) and the polymer (PANIS) was resuspended in ultrapure water and freeze-dried. The PANIS polymer was also modified with TESPIC through a hydrogen-transfer nucleophilic addition reaction to allow their grafting to the surface of AuMSS nanospheres [14]. For that purpose, PANIS (200 mg) was dissolved in 60 mL of THF under a nitrogen atmosphere and magnetic stirring. After 6 h at 60 °C, 100 μL of TESPIC were added to the mixture and left to react for 24 h. The PANIS silane derivative (TPANIS) was recovered by evaporation (Rotavap®R-215, Büchi, Switzerland), purified by dialysis in ultrapure water, and freeze-dried. The successful synthesis of TPANIS was confirmed by using the Fourier-transform infrared spectroscopy (FTIR) analysis using a Nicolet iS10 spectrometer (Thermo Scientific Inc., MA, USA).

2.2.5. AuMSS functionalization

The TPANIS was chemically linked to the AuMSS surface by using a post-synthesis grafting methodology as previously described in the literature [38]. For that purpose, a TPANIS solution (1 mg/mL in EtOH 33% *v*/v, at pH 4) was added to AuMSS nanospheres (polymer/nanospheres ratio 3:1) and stirred for 24 h (Fig. S1). After this period, AuMSS-TPANIS nanoparticles were centrifuged (6000 *g* for 25 min at 25 °C) and washed several times with ultrapure water to remove unlinked polymer chains.

2.2.6. Characterization of the AuMSS nanoformulations' physicochemical properties

The size and charge of AuMSS and AuMSS-TPANIS nanospheres were determined using a ZetaSizer NanoZS (Malvern Instruments Ltd., United Kingdom). Further, preliminary stability assays were performed by assessing the variation in the size distribution of nanospheres dispersed in ultrapure water for 24 h. In turn, the morphology and core-shell organization of AuMSS and AuMSS-TPANIS nanospheres was characterized by using Transmission Electron Microscope (TEM - Hitachi-HT7700, Japan) operated at an accelerating voltage of 80 kV or 200 kV. FTIR spectroscopy was used to evaluate both the successful removal of CTAB and the grafting of the TPANIS polymer. FTIR spectra of AuMSS and AuMSS-TPANIS were acquired with a spectral resolution of 4 cm^{-1} ranging from 4000 cm^{-1} to 600 cm^{-1} in a Nicolet iS10 spectrometer (Thermo Scientific Inc., USA). Moreover, the amount of TPANIS grafted on the AuMSS nanospheres was measured by Thermogravimetric analysis (TGA). Briefly, the weight losses AuMSS and AuMSS-TPANIS nanospheres were recorded upon heating up to 600 °C under an inert atmosphere on an SDT Q600 equipment (TA Instruments, USA).

2.2.7. Drug loading

The DOX and AO loading in AuMSS and AuMSS-TPANIS nanospheres was accomplished through an impregnation method [14]. For that purpose, AuMSS and AuMSS-TPANIS nanospheres were resuspended in 10 mL of methanol containing DOX or AO (200 μg/mL) and stirred for 48 h at room temperature. Then, the nanospheres were recovered by centrifugation (18,000 *g* for 20 min at 4 °C) and the supernatant used to determine the loading of AO and DOX. Briefly, supernatant absorbance at 485 nm for DOX and 489 nm for AO was measured using an Ultraviolet-visible (UV–vis) Spectrophotometer (Thermo Scientific Evolution™ 201 Bio UV–Vis Spectrophotometer, Thermo Fisher Scientific Inc., USA). The drug concentration was then calculated using a calibration curve (DOX - Abs = 0.0162C-0.001; R^2 = 0.999; AO - Abs = 0.1981C–0.0033; R^2 = 0.999). The encapsulation efficiency (E.E) was calculated using Eq. (2):

$$\text{E.E.}(\%) = \frac{(\text{Initial drug weight} - \text{Drug weight in the supernatant})}{\text{Initial drug weight}} \times 100 \quad (2)$$

2.2.8. Evaluation of AuMSS nanoparticles' cytocompatibility

The cytocompatibility of AuMSS and AuMSS-TPANIS nanospheres was evaluated on cancer (HeLa and MCF-7) and normal cells (FibH) using a resazurin-based assay [40]. Briefly, 96-well flat-bottom culture plates were seeded with the different cell lines at a density of 10,000 cells/well and cultured for 24 h at 37 °C in an incubator with a humidified atmosphere containing 5% CO_2. Then, the culture medium was replaced, and the cells were incubated with different concentrations of nanospheres, ranging from 25 to 200 μg/mL for 24, 48, and 72 h. At each time point, the cells were incubated with a resazurin solution for 4 h at 37 °C and 5% CO_2. Then, the cells' viability was determined by measuring the resorufin fluorescence, as described above. Cells incubated with EtOH (99.9%) and cells only incubated with culture medium were used as positive (K^+) and negative (K^-) controls, respectively.

2.2.9. Evaluation of nanoparticles' cellular uptake

The AuMSS and AuMSS-TPANIS nanospheres targeting capacity and uptake by FibH, HeLa, and MCF-7 cells were determined by fluorescence spectroscopy, through a method described by Reis and colleagues [38]. Briefly, 96-well flat-bottom culture plates were seeded with the different cell lines and cultured for 24 h at 37 °C and 5% CO_2. Then, the cells were incubated with the FTIC-labelled AuMSS or AuMSS-TPANIS nanoparticles at 200 μg/mL for 4 h. Further, one of the test groups was previously treated with free ANIS (10 μg/mL) for 3 h. Afterwards, the cells were washed with ice-cold Krebs Ringer Buffer (KRB) to remove the non-internalized particles and lysed with 1% Triton X-100 in KRB for 30 min at 37 °C. The FITC fluorescence was quantified with a spectrofluorometer (Spectramax Gemini XS, Molecular Devices LLC, USA) at an excitation/emission wavelength of λex = 480 nm and λem = 570 nm. Cells only incubated with KRB were used as a negative control.

2.2.10. Characterization of 2D cell cytotoxicity profile AuMSS-TPANIS

The cytotoxic effect of the AO or DOX-loaded AuMSS-TPANIS nanospheres was evaluated on HeLa and MCF-7 cells, through the resazurin assay. For that purpose, HeLa or MCF-7 cancer cells were seeded in 96-well flat-bottom culture plates at a density of 10,000 cells/well and cultured for 24 h at 37 °C and 5% CO_2. After 24 h, cells were incubated with AO or DOX-loaded AuMSS-TPANIS nanospheres (200 μg/mL, with DOX/AO ratios of 2:1, 1:1, and 1:2) for 48 h. Afterwards, the viability of HeLa and MCF-7 cells was measured by using the resazurin assay as previously described. Cells incubated with EtOH (99.9%) and cells only incubated with culture medium were used as positive (K^+) and negative (K^-) controls, respectively.

2.2.11. Statistical analysis

All data are presented as the mean ± standard deviation (s.d.). The statistical analysis was performed using One-way ANOVA test. A value of p lower than 0.05 ($p < 0.05$) was considered statistically significant. The statistical analysis was performed using GraphPad Prism v.7.0 software (GraphPad Software, USA).

3. Results and discussion

3.1. Evaluation of DOX:AO drug combination

To evaluate the effect of the DOX:AO combination towards cancer cells, an initial screening of the DOX and AO therapeutic capacity was performed in HeLa and MCF-7 cancer cells (Fig. 1). With that in mind,

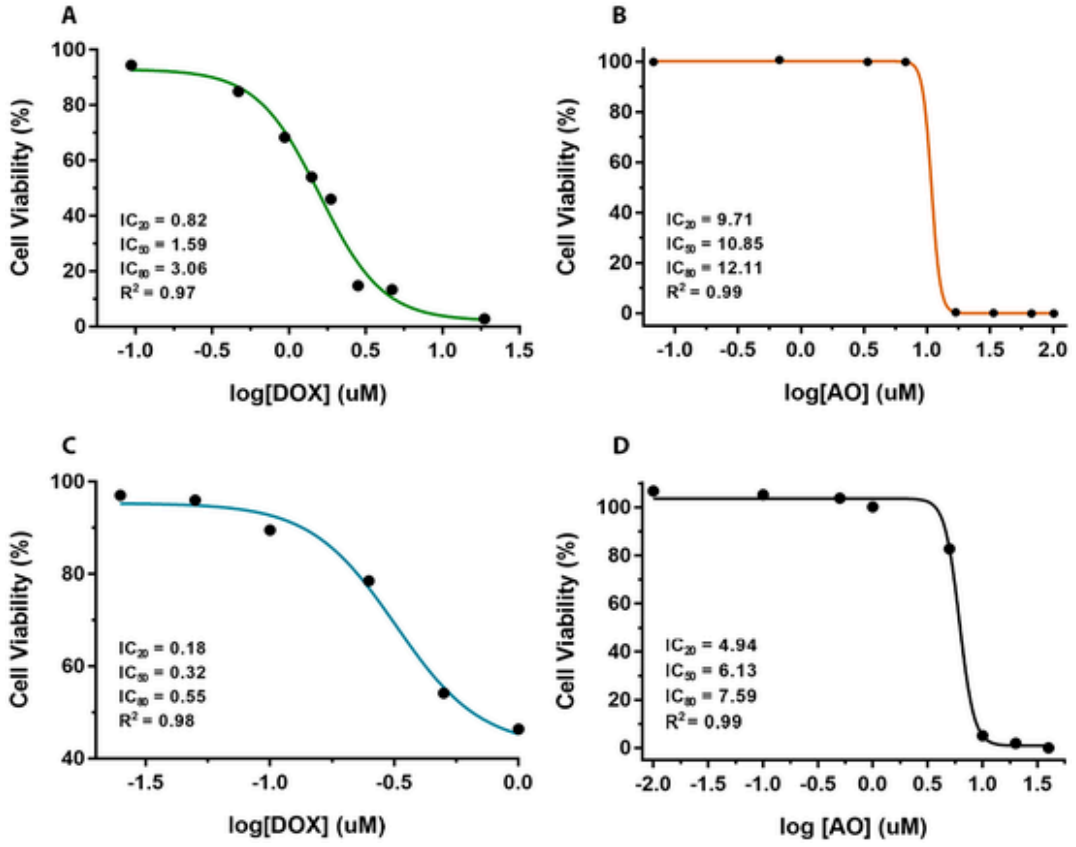

Fig. 1. Evaluation of the DOX and AO therapeutic capacity in HeLa and MCF-7 cancer cells. Dose-response curves of DOX (A) and AO (B) in HeLa Cells. Dose-response curves of DOX (C) and AO (D) in MCF-7 cells.

the cancer cells were incubated 48 h with crescent drug concentrations and the cancer cells' viability was determined. The obtained results were used to calculate the dose-effect curves and IC values (*i.e.* IC_{20}, IC_{50}, IC_{80}). In Fig. 1, it is possible to observe that the DOX display a higher cytotoxic effect in HeLa and MCF-7 cells than AO. In fact, the IC_{50} of DOX was about 6.8-times lower than that of AO in HeLa cells (IC_{50} (DOX) = 1.59 μM; IC_{50} (AO) = 10.85 μM) and 19-times lower in MCF-7 cells (IC_{50} (DOX) = 0.32 μM; IC_{50} (AO) = 6.12 μM.

After determining the DOX and AO ICs values in HeLa and MCF-7 cancer cells, a preliminary screening of the DOX:AO therapeutic efficacy was performed on HeLa cells (Fig. S2). For that purpose, HeLa cancer cells were incubated with different DOX:AO ratios (5:1 to 1:5) at a total drug concentration of 0.82, 1.59, and 3.06 μM, which correspond to the IC_{20}, IC_{50}, and IC_{80} of DOX. Further, to compare the effect of the DOX:AO drug combination, the HeLa cancer cells' response to equivalent DOX concentrations (monotherapy) was also studied. The obtained results show that a superior cytotoxic effect can be obtained with the DOX:AO drug combination when compared to the single DOX administration, principally at concentrations higher than the IC_{20} (0.82 μM). Moreover, considering the three tested concentrations in general, the DOX:AO drug ratios of 2:1, 1:1, and 1:2 display the most effective anticancer effect against the HeLa cancer cells, presenting the lowest cell viability from the tested groups. These results show the advantage of the DOX:AO drug combination, allowing the application of lower doses of DOX, which can decrease both the therapy cost and the side effects (*e.g.* cardiotoxicity, hepatotoxicity, and nephrotoxicity) [22,41]. Afterwards, the HeLa and MCF-7 cells dose-response curves were traced to determine the IC_{20}, IC_{50}, and IC_{80} of 2:1, 1:1, and 1:2 DOX:AO drug ratios (Fig. 2). As expected, the IC values of the DOX:AO drug combinations were lower than those obtained for the single DOX administration in both cell lines.

For example, the IC_{50} for 2:1, 1:1, and 1:2 DOX:AO drug ratios in HeLa cancer cells was 0.829, 0.741, and 0.937 μM, respectively, whereas the value obtained for single DOX was 1.59 μM. Moreover, to further evaluate the therapeutic potential of DOX:AO combinations, the CI was calculated for 2:1, 1:1, and 1:2 DOX:AO drug ratios (Fig. 3) [36,37]. The results obtained for HeLa cells revealed that all the DOX:AO drug ratios induce a synergistic effect (CI values lower than 1). Otherwise, the 2:1 DOX:AO drug ratio presented an antagonistic effect in MCF-7 cells, whereas the 1:1 and 1:2 DOX:AO drug ratios resulted in synergistic effects. In a therapeutic point-of-view, it is important to highlight the possibility to tailor the DOX:AO drug combination to mediate synergistic cytotoxic effects in both cancer cell lines, reducing the drug dose necessary to eradicate the tumor [10]. This synergism may be related to DOX and AO simultaneous action over different cellular targets. The DOX intercalation with the DNA base pairs inhibits the action of type II topoisomerase and the DNA replication, such stress can lead to the breakage of DNA strands and consequent cell death [22,23]. Additionally, the DOX can also mediate the formation of reactive oxygen species that increase the cell oxidative stress, lipid peroxidation, as well as the membrane and DNA damage [22,42]. In turn, the AO and its derivatives can induce the expression and the stabilization of p53 protein and consequently the cell death *via* activation of BAX [43]. Moreover, AO can also increase the production of reactive radicals, particularly when exposed blue light (*e.g.*, 488 nm) or low doses of X-ray radiation [44].

3.2. Synthesis and characterization of TPANIS

After the selection of the DOX:AO drug combinations, the AuMSS-TPANIS nanoparticles were produced to load the DOX and AO and deliver them to cancer cells. For that purpose, the ANIS was chemically linked to PEG *via* a CDI-mediated coupling reaction [45,46]. Then, the

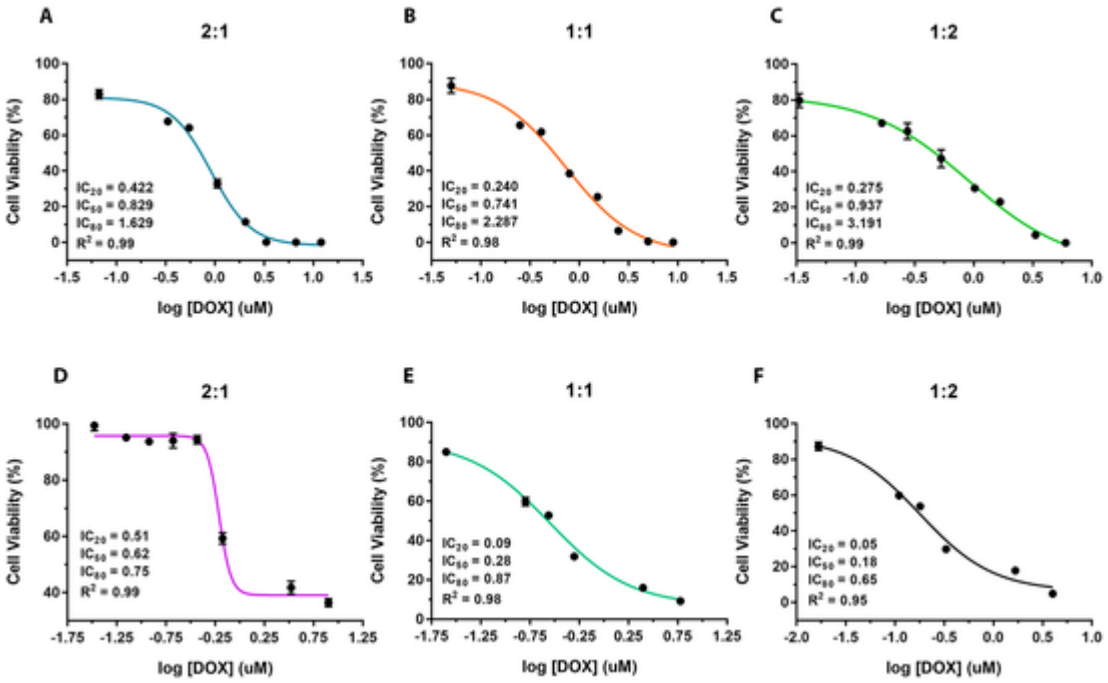

Fig. 2. Analysis of the cytotoxic effect of DOX:AO combinations in HeLa and MCF-7 cancer cells. Dose-response curves of DOX:AO at ratio 2:1 (A and D), 1:1 (B and E), and 1:2 (C and F) in HeLa (A-C) and MCF-7 (D—F) cancer cells. Data are presented as mean ± s.d., $n = 5$.

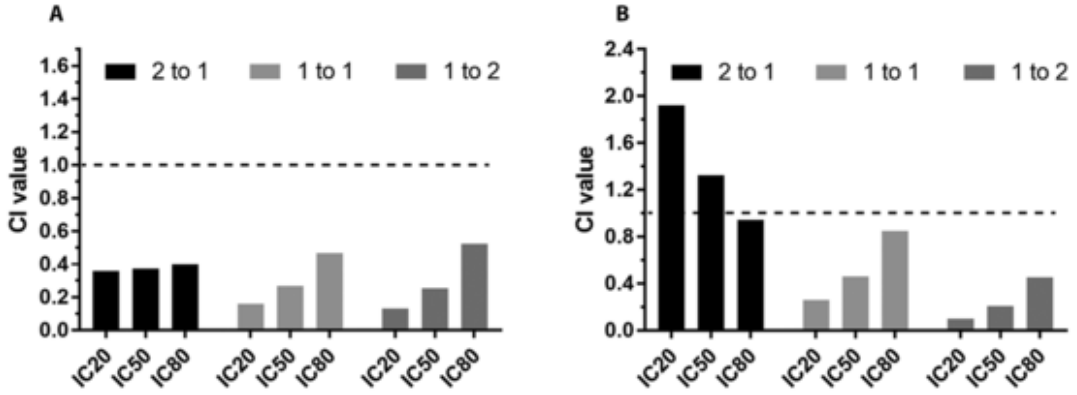

Fig. 3. Chou-Talay analysis for DOX:AO drug ratios. CI values of 2:1, 1:1, and 1:2 DOX:AO ratios in (A) HeLa and (B) MCF-7 cells. CI values of CI < 1 are considered synergistic, whereas values >1 are antagonistic effects.

resulting polymer was reacted with TESPIC (originating the TPANIS), in a hydrogen-transfer nucleophilic addition reaction, to allow its subsequent grafting to the AuMSS surface (Fig. S3 A). The TESPIC-PEG-ANIS successful modification was followed step-by-step through FTIR analysis (Fig. S3 B). The FTIR spectra of PEG present the characteristics peaks around 2800 cm^{-1} and 1000–1200 cm^{-1} region corresponding to the stretching vibrations of C—H and C—O, respectively [47]. Furthermore, the FTIR spectrum of PANIS shows both the PEG characteristic peaks and the ANIS C-O-C vibration peak in the 1500–1650 cm^{-1} region. Otherwise, the TPANIS spectrum also showed the TESPIC characteristic peaks at the 800 cm^{-1} region attributed to Si-O-C and Si—C bonds as well as the carbonyl stretches at the 1700 cm^{-1} region. In this way, this polymer can be explored to functionalize the AuMSS nanospheres increasing its colloidal stability (*i.e.* PEG) as well as the targeting towards cancer cells overexpressing sigma-1 receptors (*i.e.* ANIS) [32,34].

3.3. Synthesis and characterization of AuMSS nanospheres

The synthesis of AuMSS was performed by adapting a method previously described in the literature [38]. The AuMSS nanospheres production can be divided into two main steps, the formation of spherical gold cores and the coating with a mesoporous silica shell. Subsequently, the surfactant (*i.e.,* CTAB) is removed by a solvent extraction method using HCl [48]. Then, the AuMSS nanospheres were functionalized by a condensation reaction with the TPANIS. The morphology of functionalized and non-functionalized AuMSS nanospheres was characterized by TEM. The images confirmed the successful synthesis of spherical AuMSS composed of a gold core (darker central region of the nanoparticles) coated with a uniform mesoporous silica shell (Fig. 4 A and B) Additionally, the size data (Fig. 4 C and D) shows that the AuMSS nanospheres are homogeneous and present an average diameter of 117.2 ± 1.7 nm, and after the functionalization with TPANIS the AuMSS nanospheres overall size increased to 192.6 ± 2.9 nm. On the other side, the surface charge of AuMSS nanoformulations was also measured to characterize the surface functionalization of the nanoparticles (Fig. 5 A). The obtained results show that the non-coated AuMSS

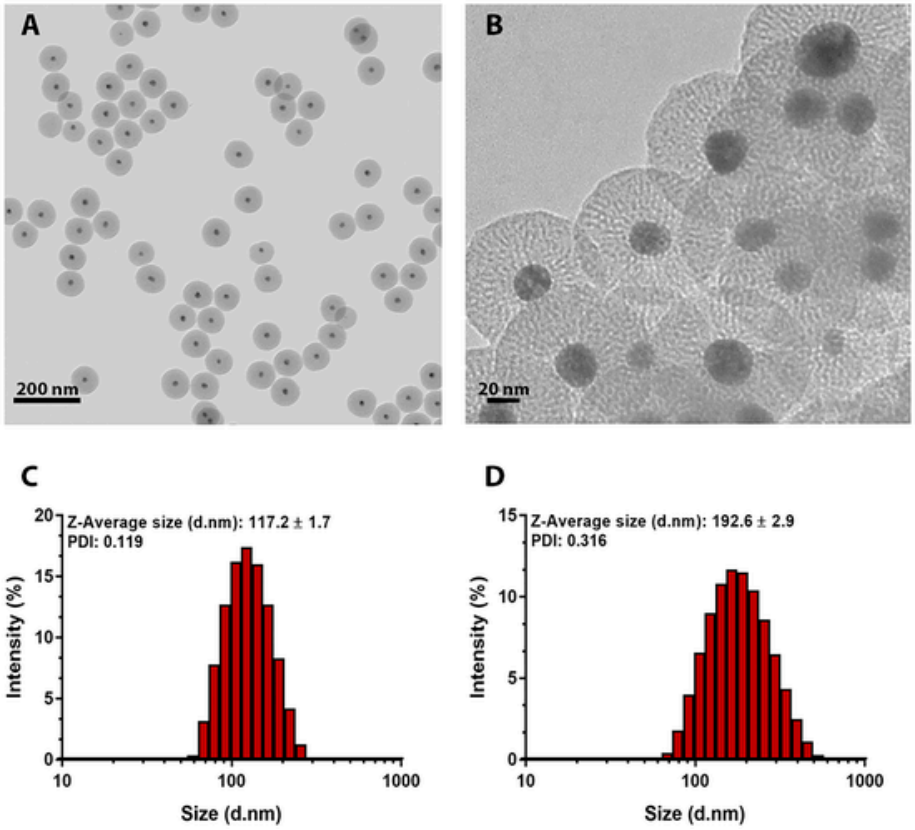

Fig. 4. Analysis of the morphology and size distribution of the AuMSS nanoformulations. TEM images of AuMSS (A) and AuMSS-TPANIS (B) nanospheres. Size distribution of AuMSS (C) and AuMSS-TPANIS (D) nanospheres. Data are presented as mean ± s.d., $n = 3$.

nanospheres display a zeta potential of - 28.1 ± 0.6 mV, whereas the AuMSS-TPANIS presents a slightly less negative surface charge, −24.7 ± 0.4 mV. These results indicate the successful grafting of TPANIS on the surface of AuMSS nanospheres.

Further, it is important to notice that the obtained mean sizes are still within the range considered ideal for application in blood circulation, allowing the nanoparticles to take advantage of the EPR effect, which consequently enables their passive accumulation in the tumor tissue tumor [48]. Moreover, despite a neutral surface charge (zeta potential of ±10 mV) often being considered the ideal for biological applications, slightly negative nanoparticles usually presented increased blood circulation times, since their interactions with blood cellular components and serum proteins are decreased [49,50].

The FTIR characterization of the AuMSS nanoformulations was carried out for assessing the formation of the mesoporous silica coating, the efficacy of the purification procedure, and the successful functionalization with TPANIS (Fig. 5 B). The FTIR spectra of AuMSS shows three characteristic peaks of mesoporous silica in 1300 to 740 cm^{-1} region that corresponds to Si-O-Si, Si-OH, and Si—O vibrations. Further, the non-purified AuMSS also presents the characteristic peaks of CTAB, namely the C—H stretching vibrations observed at 2923 and 2855 cm^{-1}. After the purification procedure, the previous C—H peaks attributed to CTAB completely disappeared, which indicates the complete removal of the cytotoxic CTAB molecules. Otherwise, after the grafting of TPANIS to the AuMSS nanospheres, it was possible to observe the presence of additional peaks corresponding to the TPANIS polymer, such as the stretching vibrations of C—H at ≈2800 cm^{-1} and C-O-C vibration peaks in the 1500–1650 cm^{-1} region. Additionally, the AuMSS-TPANIS polymeric content was determined by TGA, as shown in Fig. 5 C. As expected, the weight losses registered for non-coated AuMSS nanospheres were minimal (3–4%). Such is justified by the inorganic nature of AuMSS nanospheres and this small weight change can be attributed to the loss of the hydroxyl groups on the external surface of the particles or the evaporation of water adsorbed in the interior region of the mesopores. On the other side, the AuMSS-TPANIS presented a weight loss of 24% due to the polymer pyrolysis. To further assess the advantages of the TPANIS coating, size analysis was performed to the different AuMSS formulations after dispersion in water for different periods (Fig. 5 D). The obtained results demonstrate that the AuMSS-TPANIS present a similar size and no signs of aggregation were detected during the experiment. Contrarily, the non-coated AuMSS nanospheres showed a significant size increase from ≈115 to ≈165 nm after 24 h of incubation in water. Overall, the different physicochemical results corroborate the successful immobilization of TPANIS on the AuMSS surface.

3.4. Drug loading capacity of AuMSS and AuMSS-TPANIS

The AuMSS capacity to encapsulate chemotherapeutic drugs was characterized by measuring the E.E of DOX and AO. The loading was promoted by resuspending the AuMSS nanospheres in the DOX or AO solution for 48 h (Fig. 6 A). The obtained results showed that all the AuMSS formulations can encapsulate the two drugs. The non-coated AuMSS nanospheres presented an E.E of 92% for DOX and 48% for AO (Fig. 6 B). Otherwise, the AuMSS-TPANIS nanospheres presented a slightly higher E.E, 97% for DOX, and 53% for AO. The drug loading in the AuMSS nanoparticles is mediated by the establishment of electrostatic and/or hydrophobic interactions between the drug molecules and the silica mesopores. The increase in the E.E with the TPANIS functionalization can be justified by the additional entrapment of drug molecules at the particle surface promoted by the TPANIS polymer as reported in the literature for similar strategies [14]. Furthermore, the release assays (Fig. S4) demonstrated that the drug release is independent on the pH value of the outer media (*i.e.*, 7.4 or 5.6). Moreover, the TPA-

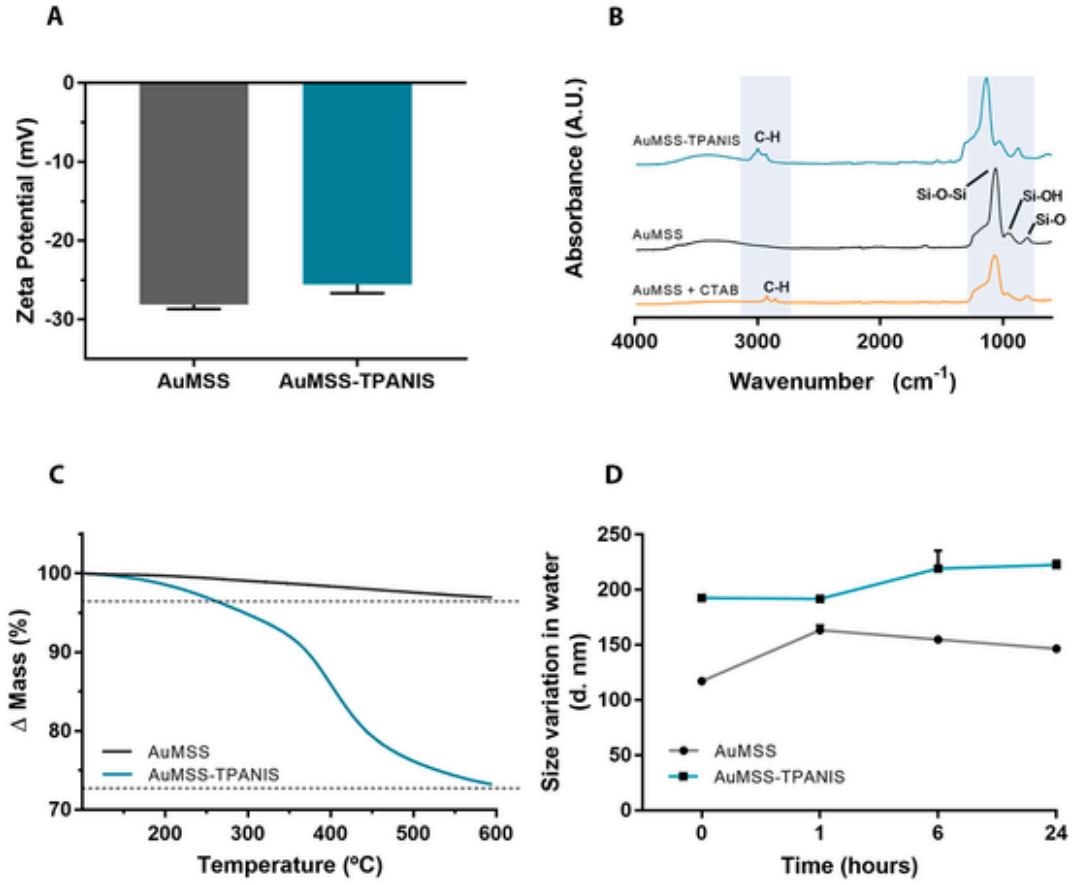

Fig. 5. Physicochemical characterization of AuMSS nanoformulations. (A) Surface charge analysis of AuMSS and AuMSS-TPANIS nanospheres, $n = 3$. (B) FTIR spectra of non-purified AuMSS (AuMSS + CTAB), AuMSS, and AuMSS-TPANIS nanospheres. (C) TGA analysis of AuMSS and AuMSS-TPANIS nanospheres. (D) Size variation of AuMSS and AuMSS-TPANIS nanospheres when dispersed in ultrapure water for 24 h. Data are presented as mean ± s.d., n = 3.

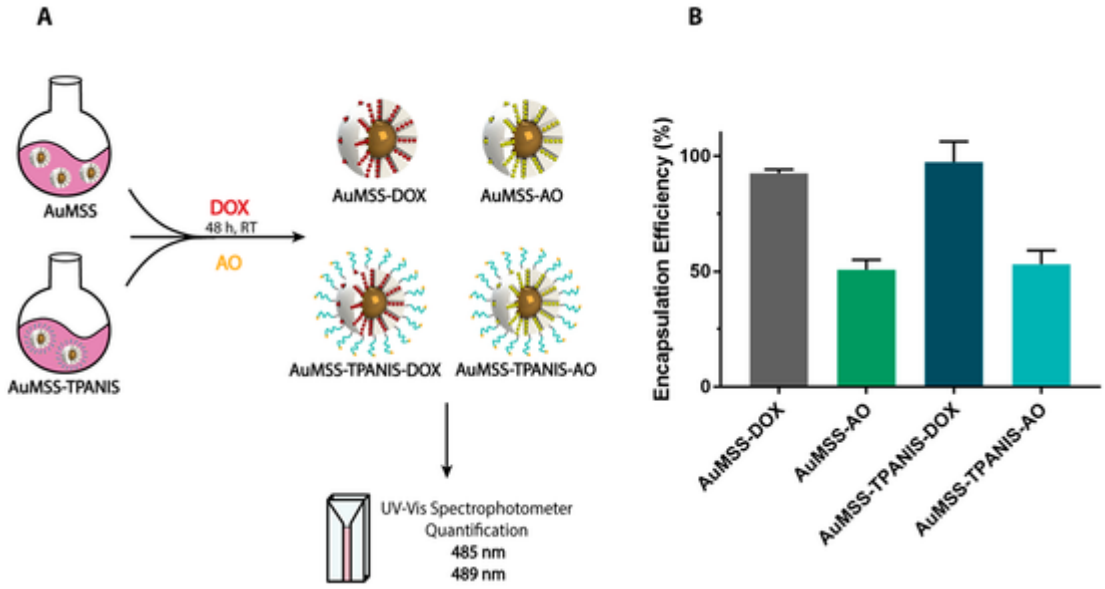

Fig. 6. Characterization of the DOX and AO encapsulation efficiency. (A) Schematics of DOX or AO loading in AuMSS and AuMSS-TPANIS nanoparticles. (B) DOX and AO encapsulation efficiency on AuMSS and AuMSS-TPANIS nanospheres. Data are presented as mean ± s.d, $n = 3$.

NIS functionalization results in a slower drug release from the AuMSS nanospheres than the non-coated counterparts, ≈45% and ≈90% of drug released at 48 h of incubation, respectively. Such can be attributed to the TPANIS outer layer on the functionalized AuMSS nanos-

pheres, which provides an additional barrier delaying the drug diffusion from the silica mesopores.

3.5. Nanoparticles cytocompatibility

The cytocompatibility of AuMSS and AuMSS-TPANIS nanospheres was evaluated in HeLa, MCF-7, and FibH cells through the resazurin assay. For that purpose, the two different AuMSS formulations were incubated with the cells for 24, 48, and 72 h, at concentrations ranging from 25 to 200 μg/mL (Fig. 7).

According to the ISO 10993-5, a material has a cytotoxic effect when the cell viability suffers a reduction of more than 30% [51,52]. The obtained results reveal that both the AuMSS and AuMSS-TPANIS nanospheres did not induce a cytotoxic effect in the three tested cell lines, registering cell viabilities higher than 70%, even at the highest concentration (200 μg/mL). These results are in agreement with the data available in the literature for AuMSS-based nanosystems and the safety profile of PEG (FDA-approved for biomedical applications) [14,38,53].

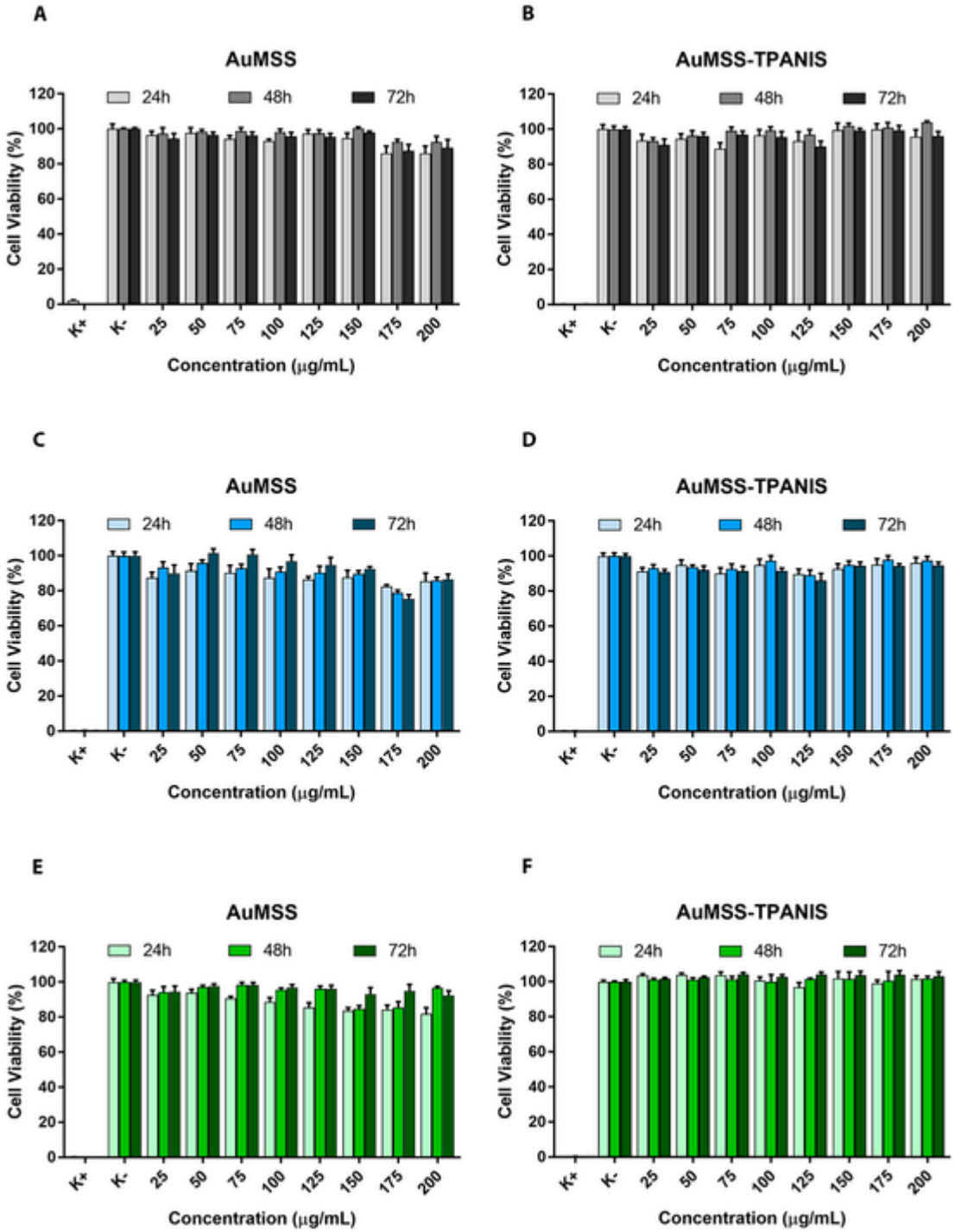

Fig. 7. Evaluation of AuMSS and AuMSS-TPANIS cytocompatibility in HeLa (A, B), MCF-7 (C, D) and FibH (E, F) at 24, 48, and 72 h. Positive control (K^+): cells treated with EtOH; Negative control (K^-): cells without nanoparticles incubation. Data are presented as mean ± s.d., $n = 5$.

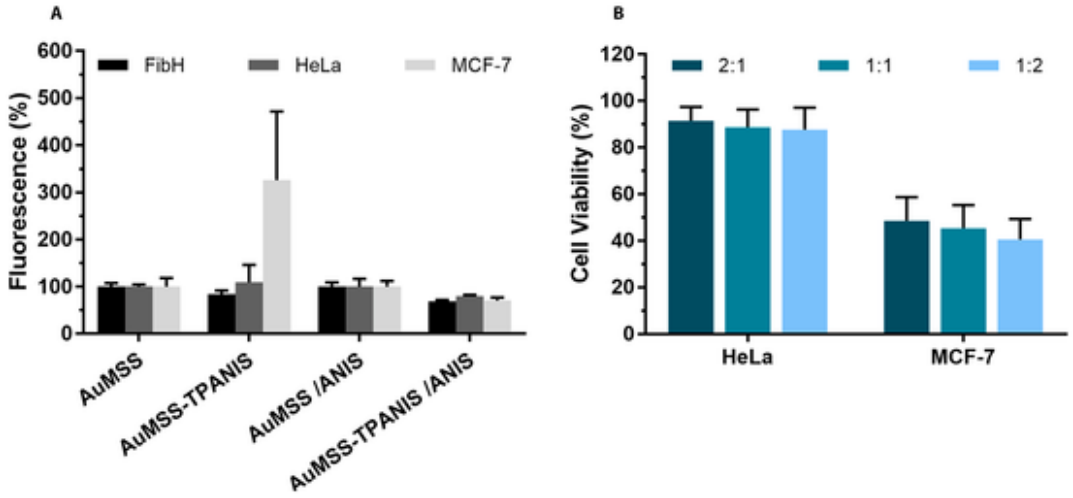

Fig. 8. Analysis of AuMSS and AuMSS-TPANIS therapeutic potential. (A) Fluorescence spectroscopy analysis of the AuMSS and AuMSS-TPANIS uptake by FibH, HeLa, and MCF-7 cells with or without pre-treatment with ANIS. (B) Cytotoxic activity of AuMSS-TPANIS nanospheres at DOX:AO ratio of 2:1, 1:1, and 1:2. Data are presented as mean ± s.d., $n = 5$.

3.6. AuMSS spheres cellular uptake

After assessing the biocompatibility of AuMSS nanoformulations, the nanoparticles' cellular uptake was evaluated by fluorescence spectroscopy. For that purpose, FITC-stained AuMSS and AuMSS-TPANIS nanospheres were incubated with FibH (healthy cells with low expression of sigma receptors), HeLa (cancer cells with low expression of sigma receptors), and MCF-7 (cancer cells overexpressing sigma receptors) cells for 4 h (Fig. 8 A). These different cell lines were selected to evaluate the ANIS targeting ability. The fluorescence spectroscopy studies revealed that the AuMSS nanospheres functionalization with TPANIS improves the nanoparticle uptake in MCF-7 cancer cells, 326 ± 119% when compared to non-coated AuMSS nanospheres. Otherwise, in HeLa and FibH cells, the AuMSS-TPANIS presented an uptake similar to non-coated AuMSS nanospheres. This enhanced AuMSS-TPANIS uptake in MCF-7 cells indicates that the nanoparticle internalization may be mediated by the ANIS interaction with the sigma receptors overexpressed in this cell line. With that in mind, the uptake experiments were repeated by performing the pre-treatment of FibH, HeLa, and MCF-7 cells with free ANIS for 3 h before the nanoparticle incubation. The obtained data demonstrated that the pre-treatment with ANIS reverts the AuMSS-TPANIS increased uptake by MCF-7 cells, registering a similar fluorescence value in the 3 tested cell lines. Therefore, this experiment demonstrated that the introduction of TPANIS in the AuMSS nanospheres confer to the nanoparticles an increased selectivity towards cancer cells overexpressing the sigma receptors, such as breast cancer, melanoma, and prostate cancer, as observed in the literature in different nanomaterials [31,54,55].

3.7. Cytotoxic effect of loaded AuMSS-TPANIS spheres

The anti-cancer potential of DOX or AO loaded AuMSS-TPANIS nanospheres was evaluated both in HeLa and MCF-7 cells. For that purpose, the cancer cells were incubated with different ratios of drug-loaded AuMSS-TPANIS nanospheres (maximum nanoparticle concentration of 200 μg/mL corresponding to DOX:AO drug ratios of 2:1, 1:1, and 1:2) for 48 h. The obtained results (Fig. 8 B) show that the AuMSS-TPANIS nanospheres have a superior cytotoxic effect on MCF-7 cells, 49%, 45%, and 41% of viable cells for the DOX:AO ratio of 2:1, 1:1, and 1:2, respectively. In contrast, the HeLa cells presented viabilities around 90% after the treatment with drug-loaded AuMSS-TPANIS nanospheres. However, when compared to the data obtained with the free DOX:AO (Fig. 2), the drug-loaded AuMSS-TPANIS presented lower cytotoxicity. Such can be justified by the release profile, only 45% of AuMSS-TPANIS drug content is released in the 48 h of the study. Additionally, the differences observed between the AuMSS-TPANIS nanospheres' cytotoxicity in HeLa and MCF-7 cells corroborate the efficacy of the ANIS-mediated active targeting towards sigma receptors MCF-7 cancer cells. The preferential and faster nanoparticle uptake in the MCF-7 cells maximize the drug dose that reaches the cell cytoplasm and consequently enhance the therapeutic potential of AuMSS-TPANIS nanospheres.

4. Conclusion

Currently, chemotherapy is one of the most explored anticancer approaches in clinical practice. Nevertheless, chemotherapeutic drugs present several disadvantages that affect their therapeutic outcome. Thus, there is a huge demand to develop novel and more effective therapeutic approaches that are able to improve the efficacy of anticancer treatments. Combinatorial therapies based on the simultaneous administration of multiple drugs intend to overcome the limitations of conventional chemotherapy by targeting simultaneously different metabolic pathways or administering complementary drugs to create additive or synergetic effects that potentiate the therapeutic efficacy even at smaller drug doses. In this work, a dual drug combination (DOX and AO) was explored to be encapsulated in AuMSS nanospheres. Moreover, a novel AuMSS surface modification based on TPANIS was developed to improve nanoparticles' blood circulation time and specificity to cancer cells, namely those overexpressing sigma receptors. The obtained results demonstrated that the DOX:AO drug combination can mediate a synergistic therapeutic effect in both HeLa and MCF-7 cells, particularly at the 2:1, 1:1, and 1:2 ratios. Otherwise, AuMSS nanoparticles' functionalization with the TPANIS promoted a slight increase in the nanoparticles' size and colloidal stability. Additionally, both the DOX and AO were successfully encapsulated on the AuMSS-TPANIS nanospheres. Moreover, the AuMSS nanospheres' functionalization with TPANIS significantly increased their internalization by MCF-7 cells (cells overexpressing sigma receptors). This selectivity towards MCF-7 cells also resulted in an enhanced cytotoxic effect. Overall, the obtained results demonstrated the therapeutic potential of the DOX:AO drug combination as well as the targeting capacity of AuMSS-TPANIS nanospheres, which supports its development for anti-cancer or other biomedical applications.

CRediT authorship contribution statement

Rafaela S. Guimarães: Conceptualization, Methodology, Investigation. **Carolina F. Rodrigues:** Methodology, Investigation, Writing - original draft. **Natanael Fernandes:** Conceptualization, Investigation. **Duarte de Melo-Diogo:** Visualization, Writing - original draft. **Paula Ferreira:** Investigation. **Ilídio J. Correia:** Supervision, Writing - review & editing. **André F. Moreira:** Conceptualization, Writing - original draft, Writing - review & editing.

Declaration of Competing Interest

The authors declare no financial or commercial conflict of interest.

Acknowledgements

This work was financed by the Foundation for Science and Technology (FCT), through funds from the State Budget, and by the European Regional Development Fund (ERDF), under the Portugal 2020 Program, through the Regional Operational Program of the Center (Centro2020), through the Project with the reference UIDB / 00709/2020. The funding from CENTRO-01-0145-FEDER-028989 and POCI-01-0145-FEDER-031462 are also acknowledged. Carolina F. Rodrigues acknowledge for her Ph.D. fellowship from FCT (SFRH/BD/144680/2019). The funders had no role in the decision to publish or in the preparation of the manuscript.

Appendix A. Supplementary data

Supplementary data to this article can be found online at https://doi.org/10.1016/j.jinorgbio.2021.111433.

References

[1] R.L. Siegel, K.D. Miller, A. Jemal, Cancer statistics, 2019, CA Cancer J. Clin. 69 (1) (2019) 7–34.
[2] F. Bray, et al., Global cancer statistics 2018: GLOBOCAN estimates of incidence and mortality worldwide for 36 cancers in 185 countries, CA Cancer J. Clin. 68 (6) (2018) 394–424.
[3] M. Chidambaram, R. Manavalan, K. Kathiresan, Nanotherapeutics to overcome conventional cancer chemotherapy limitations, J Pharm Pharm Sci 14 (1) (2011) 67–77.
[4] Q. Hu, et al., Recent advances of cocktail chemotherapy by combination drug delivery systems, Adv. Drug Deliv. Rev. 98 (2016) 19–34.
[5] C. Riganti, M. Contino, New strategies to overcome resistance to chemotherapy and immune system in cancer, Int. J. Mol. Sci. 20 (19) (2019) 4783.
[6] C. Holohan, et al., Cancer drug resistance: an evolving paradigm, Nat. Rev. Cancer 13 (10) (2013) 714–726.
[7] R. Bayat Mokhtari, et al., Combination therapy in combating cancer, Oncotarget 8 (23) (2017) 38022–38043.
[8] B. Al-Lazikani, U. Banerji, P. Workman, Combinatorial drug therapy for cancer in the post-genomic era, Nat. Biotechnol. 30 (7) (2012) 679–692.
[9] A.C. Palmer, P.K. Sorger, Combination cancer therapy can confer benefit via patient-to-patient variability without drug additivity or synergy, Cell 171 (7) (2017) 1678–1691 e13.
[10] R.X. Zhang, et al., Nanomedicine of synergistic drug combinations for cancer therapy – strategies and perspectives, J. Control. Release 240 (2016) 489–503.
[11] C.-M.J. Hu, L. Zhang, Nanoparticle-based combination therapy toward overcoming drug resistance in cancer, Biochem. Pharmacol. 83 (8) (2012) 1104–1111.
[12] S.-Y. Qin, et al., Combinational strategy for high-performance cancer chemotherapy, Biomaterials 171 (2018) 178–197.
[13] S. Kapse-Mistry, et al., Nanodrug delivery in reversing multidrug resistance in cancer cells, Front. Pharmacol. 5 (2014) 159–159.
[14] A.F. Moreira, et al., Development of poly-2-ethyl-2-oxazoline coated gold-core silica shell nanorods for cancer chemo-photothermal therapy, Nanomedicine 13 (20) (2018) 2611–2627.
[15] C.F. Rodrigues, et al., Functionalization of AuMSS nanorods towards more effective cancer therapies, Nano Res. 12 (4) (2019) 719–732.
[16] A.F. Moreira, et al., Gold-core silica shell nanoparticles application in imaging and therapy: a review, Microporous Mesoporous Mater. 270 (2018) 168–179.
[17] K. Hayashi, et al., Gold nanoparticle cluster-plasmon-enhanced fluorescent silica core-shell nanoparticles for X-ray computed tomography-fluorescence dual-mode imaging of tumors, Chem. Commun. (Camb.) 49 (46) (2013) 5334–5336.
[18] S. Jafari, et al., Mesoporous silica nanoparticles for therapeutic/diagnostic applications, Biomed. Pharmacother. 109 (2019) 1100–1111.
[19] A.-V. Tran, et al., Targeted and controlled drug delivery by multifunctional mesoporous silica nanoparticles with internal fluorescent conjugates and external polydopamine and graphene oxide layers, Acta Biomater. 74 (2018) 397–413.
[20] R.R. Castillo, et al., Advances in mesoporous silica nanoparticles for targeted stimuli-responsive drug delivery: an update, Exp. Opin. Drug Deliv. 16 (4) (2019) 415–439.
[21] T.A. Jacinto, et al., Hyaluronic acid and vitamin E polyethylene glycol succinate functionalized gold-core silica shell nanorods for cancer targeted photothermal therapy, Colloids Surf. B: Biointerfaces 188 (2020) 110778.
[22] C.F. Thorn, et al., Doxorubicin pathways: pharmacodynamics and adverse effects, Pharmacogenet. Genomics 21 (7) (2011) 440–446.
[23] H. Zhu, et al., Doxorubicin redox biology: redox cycling, topoisomerase inhibition, and oxidative stress, Reactive Oxygen Spec. (Apex, N.C.) 1 (3) (2016) 189–198.
[24] K. Kusuzaki, et al., Acridine Orange could be an innovative anticancer agent under photon energy, In vivo 21 (2007) 205–214.
[25] Y.-C. Lin, et al., Acridine orange exhibits photodamage in human bladder cancer cells under blue light exposure, Sci. Rep. 7 (1) (2017) 14103.
[26] E. Iessi, et al., Acridine Orange/exosomes increase the delivery and the effectiveness of Acridine Orange in human melanoma cells: a new prototype for theranostics of tumors, J. Enzyme Inhibit. Med. Chem. 32 (1) (2017) 648–657.
[27] M. Bragagni, et al., Synthesis of an acridine orange sulfonamide derivative with potent carbonic anhydrase IX inhibitory action, J Enzyme Inhib Med Chem 32 (1) (2017) 701–706.
[28] A. Pitchaimani, et al., Photochemotherapeutic effects of UV-C on acridine orange in human breast cancer cells: potential application in anticancer therapy, RSC Adv. 4 (42) (2014) 22123.
[29] C.H. Liu, S.L. Sahoo, M.H. Tsao, Acridine orange coated magnetic nanoparticles for nucleus labeling and DNA adsorption, Colloids Surf. B: Biointerfaces 115 (2014) 150–156.
[30] K.A. Fitzgerald, et al., A novel, anisamide-targeted cyclodextrin nanoformulation for siRNA delivery to prostate cancer cells expressing the sigma-1 receptor, Int. J. Pharm. 499 (1) (2016) 131–145.
[31] L. Wang, et al., Development of anisamide-targeted PEGylated gold nanorods to deliver epirubicin for chemo-photothermal therapy in tumor-bearing mice, Int. J. Nanomedicine 14 (2019) 1817–1833.
[32] E. Aydar, et al., The expression and functional characterization of sigma (σ) 1 receptors in breast cancer cell lines, Cancer Lett. 242 (2) (2006) 245–257.
[33] B. Pelaz, et al., Surface functionalization of nanoparticles with polyethylene glycol: effects on protein adsorption and cellular uptake, ACS Nano 9 (7) (2015) 6996–7008.
[34] J.S. Suk, et al., PEGylation as a strategy for improving nanoparticle-based drug and gene delivery, Adv. Drug Deliv. Rev. 99 (2016) 28–51.
[35] A.S. Barros, et al., Comparative study of the therapeutic effect of doxorubicin and resveratrol combination on 2D and 3D (spheroids) cell culture models, Int. J. Pharm. 551 (1–2) (2018) 76–83.
[36] D. de Melo-Diogo, et al., POxylated graphene oxide nanomaterials for combination chemo-phototherapy of breast cancer cells, Eur. J. Pharm. Biopharm. 131 (2018) 162–169.
[37] T.C. Chou, Drug combination studies and their synergy quantification using the Chou-Talalay method, Cancer Res. 70 (2) (2010) 440–446.
[38] C.A. Reis, et al., Development of gold-core silica shell nanospheres coated with poly-2-ethyl-oxazoline and beta-cyclodextrin aimed for cancer therapy, Mater. Sci. Eng. C 98 (2019) 960–968.
[39] D.R. Dias, A.F. Moreira, I.J. Correia, The effect of the shape of gold core–mesoporous silica shell nanoparticles on the cellular behavior and tumor spheroid penetration, J. Mater. Chem. B 4 (47) (2016) 7630–7640.
[40] C.F. Rodrigues, et al., Optimization of gold core-mesoporous silica shell functionalization with TPGS and PEI for cancer therapy, Microporous Mesoporous Mater. 285 (2019) 1–12.
[41] Y. Kalender, M. Yel, S. Kalender, Doxorubicin hepatotoxicity and hepatic free radical metabolism in rats: the effects of vitamin E and catechin, Toxicology 209 (1) (2005) 39–45.
[42] S.-Y. Kim, et al., Doxorubicin-induced reactive oxygen species generation and intracellular Ca2+ increase are reciprocally modulated in rat cardiomyocytes, Exp. Mol. Med. 38 (5) (2006) 535–545.
[43] W. Wang, et al., Acridine derivatives activate p53 and induce tumor cell death through Bax, Cancer Biol. Ther. 4 (8) (2005) 893–898.
[44] V.A. Byvaltsev, et al., Acridine orange: a review of novel applications for surgical cancer imaging and therapy, Front. Oncol. 9 (2019) 925.
[45] C. Deng, et al., A biodegradable triblock copolymer poly(ethylene glycol)-b-poly(l-lactide)-b-poly(l-lysine): synthesis, self-assembly, and RGD peptide modification, Polymer 48 (1) (2007) 139–149.
[46] F.J. Xu, et al., Spatially well-defined binary brushes of poly(ethylene glycol)s for micropatterning of active proteins on anti-fouling surfaces, Biosens. Bioelectron. 24 (4) (2008) 773–780.
[47] B.W. Chieng, et al., Poly(lactic acid)/Poly(ethylene glycol) polymer nanocomposites: effects of graphene nanoplatelets, Polymers 6 (1) (2014).

[48] A.F. Moreira, et al., Preparation of end-capped pH-sensitive mesoporous silica nanocarriers for on-demand drug delivery, Eur. J. Pharm. Biopharm. 88 (3) (2014) 1012–1025.
[49] M.J. Ernsting, et al., Factors controlling the pharmacokinetics, biodistribution and intratumoral penetration of nanoparticles, J. Control. Release 172 (3) (2013) 782–794.
[50] E. Fröhlich, The role of surface charge in cellular uptake and cytotoxicity of medical nanoparticles, Int. J. Nanomedicine 7 (2012) 5577–5591.
[51] I. Iso, 10993–5: 2009 Biological Evaluation of Medical Devices—Part 5: Tests for In Vitro Cytotoxicity, International Organization for Standardization, Geneva, 2009.
[52] C.F. Jones, D.W. Grainger, In vitro assessments of nanomaterial toxicity, Adv. Drug Deliv. Rev. 61 (6) (2009) 438–456.
[53] A. D'Souza, R. Shegokar, Polyethylene glycol (PEG): a versatile polymer for pharmaceutical applications, Expert Opin Drug Deliv 13 (9) (2016) 1257–1275.
[54] L. Lu, et al., Anisamide-decorated pH-sensitive degradable chimaeric polymersomes mediate potent and targeted protein delivery to lung cancer cells, Biomacromolecules 16 (6) (2015) 1726–1735.
[55] D. Qu, et al., Anisamide-functionalized pH-responsive amphiphilic chitosan-based paclitaxel micelles for sigma-1 receptor targeted prostate cancer treatment, Carbohydr. Polym. 229 (2020) 115498.